


# Symplasmic phloem unloading and radial post-phloem transport via vascular rays in tuberous roots of *Manihot esculenta*

## Journal Article

### Author(s):

Mehdi, Rabih; Lamm, Christian E.; Anjanappa, Ravi B.; Müdsam, Christina; Saeed, Muhammad; Klima, Janine; Kraner, Max E.; Ludewig, Frank; Knoblauch, Michael; [Gruissem, Wilhelm](#) ; Sonnewald, Uwe; Zierer, Wolfgang

### Publication date:

2019-10-15

### Permanent link:

<https://doi.org/10.3929/ethz-b-000374960>

### Rights / license:

[Creative Commons Attribution-NonCommercial 4.0 International](#)

### Originally published in:

Journal of Experimental Botany 70(20), <https://doi.org/10.1093/jxb/erz297>



RESEARCH PAPER

# Symplasmic phloem unloading and radial post-phloem transport via vascular rays in tuberous roots of *Manihot esculenta*

Rabih Mehdi<sup>1,\*</sup>, Christian E. Lamm<sup>1,\*</sup>, Ravi Bodampalli Anjanappa<sup>2</sup>, Christina Müdsam<sup>1</sup>, Muhammad Saeed<sup>1</sup>, Janine Klima<sup>1</sup>, Max E. Kraner<sup>1</sup>, Frank Ludewig<sup>1,†</sup>, Michael Knoblauch<sup>3</sup>, Wilhelm Gruissem<sup>2,4, ID</sup>, Uwe Sonnewald<sup>1</sup> and Wolfgang Zierer<sup>1,‡</sup>

<sup>1</sup> Biochemistry, Department of Biology, Friedrich-Alexander University Erlangen-Nuremberg, Staudtstraße 5, 91058 Erlangen, Germany

<sup>2</sup> Plant Biotechnology, Department of Biology, ETH Zurich, Universitätstrasse 2, 8092 Zurich, Switzerland

<sup>3</sup> School of Biological Sciences, Washington State University, Pullman, WA 99164, USA

<sup>4</sup> Advanced Plant Biotechnology Center, National Chung Hsing University, Taichung City, Taiwan

\* These authors contributed equally to this work.

† Present address: KWS Saat SE, Grimsehlstraße 31, 37574 Einbeck, Germany.

‡ Correspondence: [wolfgang.zierer@fau.de](mailto:wolfgang.zierer@fau.de)

Received 20 March 2019; Editorial decision 13 June 2019; Accepted 15 June 2019

Editor: John Lunn, Max Planck Institute of Molecular Plant Physiology, Germany

## Abstract

**Cassava (*Manihot esculenta*) is one of the most important staple food crops worldwide. Its starchy tuberous roots supply over 800 million people with carbohydrates. Yet, surprisingly little is known about the processes involved in filling of those vital storage organs. A better understanding of cassava carbohydrate allocation and starch storage is key to improving storage root yield. Here, we studied cassava morphology and phloem sap flow from source to sink using transgenic *pAtSUC2::GFP* plants, the phloem tracers esculin and 5(6)-carboxyfluorescein diacetate, as well as several staining techniques. We show that cassava performs apoplasmic phloem loading in source leaves and symplasmic unloading into phloem parenchyma cells of tuberous roots. We demonstrate that vascular rays play an important role in radial transport from the phloem to xylem parenchyma cells in tuberous roots. Furthermore, enzymatic and proteomic measurements of storage root tissues confirmed high abundance and activity of enzymes involved in the sucrose synthase-mediated pathway and indicated that starch is stored most efficiently in the outer xylem layers of tuberous roots. Our findings form the basis for biotechnological approaches aimed at improved phloem loading and enhanced carbohydrate allocation and storage in order to increase tuberous root yield of cassava.**

**Keywords:** Apoplast, cassava, CFDA, esculin, morphology, phloem, ray, starch, SUC2, symplast.

## Introduction

Cassava (*Manihot esculenta*) is a perennial woody shrub that can form up to 14 underground storage roots (Carvalho *et al.*, 2018). Those storage roots, also called tuberous roots, are rich in starch and contribute to the nutrition of over 800 million

people, making cassava one of the most important staple food crops in the world (Howeler *et al.*, 2013).

Cassava is grown in over 100 tropical and sub-tropical countries. Although the plant originates from the Amazon region of

South America (Olsen and Schaal, 1999), today it is especially important in Sub-Saharan Africa, where half of the annual global cassava yield is produced (Howeler *et al.*, 2013). Here the crop is almost exclusively grown by smallholder farmers with limited resources. Stem cuttings are used to propagate the plant, making new planting material relatively cheap and accessible. Cassava is water efficient and can withstand prolonged periods of drought, and it even grows in acidic or nutrient-poor soils (Hershey *et al.*, 2012; Howeler *et al.*, 2013). Therefore, cassava can generate reasonable yields even under suboptimal conditions, making it ideally suited for low input agriculture.

In the face of climate change, cassava might become even more important for Sub-Saharan Africa. Rising temperature and unpredictable rainfall will reduce the yield of many crops. However, with the 2030 projections for temperature and rainfall, continued cassava cultivation is predicted in all areas where it is currently grown. Because of its heat and drought tolerance, it might even be grown more widely than today (Hershey *et al.*, 2012; Jarvis *et al.*, 2012).

Cassava was domesticated over 6000 years ago (Bredeson *et al.*, 2016), but comparably little research has been done on this crop (Hershey *et al.*, 2012). Even basic processes, such as the type of photosynthesis were only elucidated recently (De Souza *et al.*, 2017; De Souza and Long, 2018; Arrivault *et al.*, 2019). Detailed information on other important processes such as, for instance, root development is currently very limited, even though the tuberous roots are cassava's main product. Two types of adventitious roots with different cellular origin are produced from stem cuttings. While the fibrous roots originate from the stem base or stem nodes, the tuberous roots are always nodally derived (Chaweewan and Taylor, 2015). Yet unknown signals initiate secondary growth of tuberous roots producing the large underground storage organs. How the tuberous roots are filled with starch and how the required carbohydrates even reach those roots is yet unclear for cassava, as well.

In tracheophytes, the vasculature is used as a conduit for signaling molecules such as plant hormones, peptides, and proteins, as well as amino acids, RNA, and carbohydrates (Turgeon and Wolf, 2009; De Schepper *et al.*, 2013; Okamoto *et al.*, 2016; Kehr and Kragler, 2018). Whereas the xylem's main function is the distribution of water and minerals throughout the plant, the phloem is required to supply heterotrophic organs (sink tissues) with photoassimilates generated in the photosynthetically active green tissues (source tissues) to ensure the maintenance of metabolic homeostasis (Lucas *et al.*, 2013). The process of sugar allocation from source to sink can be described by four distinct steps: (i) loading of carbohydrates from mesophyll cells into companion cells (CCs) of minor veins, (ii) transport through the phloem sieve elements (SEs) to sink tissues, (iii) release of the assimilates into sink cells, and (iv) post-phloem transport.

Phloem loading occurs either symplasmically via plasmodesmata or apoplasmically via proton-driven carrier proteins. Symplasmic phloem loading relies on passive diffusion into CCs or sugar trapping as polymers inside the CCs in order to maintain the hydrostatic pressure necessary for phloem transport (Turgeon, 1996; Turgeon and Medville, 1998; Rennie and Turgeon, 2009; Fu *et al.*, 2011). Apoplasmic transport considers CCs to be symplasmically isolated and thus includes

a transporter-driven loading step (Van Bel, 2003). Sucrose is transported along the concentration gradient into the phloem parenchyma apoplast by SWEET transporters and taken up into the CCs by SUC/SUT sucrose-proton cotransporters (Giaquinta, 1977; Riesmeier *et al.*, 1994; Bürkle *et al.*, 1998; Chen *et al.*, 2012).

Once in the CCs, the transport sugar is able to enter the SE network, where long-distance transport takes place (Van Bel and Kempers, 1997). According to the pressure-flow hypothesis (Münch, 1930), verified experimentally by Knoblauch *et al.* (2016), the differential accumulation of osmotic substances such as sucrose in source and sink organs generates a hydrostatic pressure gradient, which in turn leads to a mass flow through the sieve elements. With this, sugars and other solutes are transported passively by bulk flow.

Since the pressure gradient can only be sustained by a difference in osmotic potential between source and sink, phloem unloading of carbohydrates into sink tissues and post-phloem transport is one of the driving forces of long-distance transport. Similar to the loading, transport sugars may leave the SE-CC complex either symplasmically via plasmodesmata or apoplasmically via transport proteins (Turgeon and Wolf, 2009; Braun *et al.*, 2014). In case of symplasmic unloading, the distribution of photoassimilates follows the mass flow. In general, the osmotically active substances are removed by metabolization, transferred into starch or structural carbohydrates. In plants directly accumulating high levels of osmotically active sucrose, symplasmic unloading can also be facilitated by pronounced cell wall barriers between the vasculature and the storage tissue, allowing independent osmotic regulation of two apoplasmic domains as shown in sugar cane (Milne *et al.*, 2015, 2017). In contrast to this, the energy-dependent apoplasmic unloading strategy includes an active transport of carbohydrates across membranes, analogous to the apoplasmic loading scenario. However, a frequently observed feature of apoplasmic unloading is the cleavage of sucrose into hexoses in the apoplast by cell wall invertases, followed by hexose uptake into sink cells by hexose transporters (Braun *et al.*, 2014). Generally, most storage organs seem to employ a symplasmic unloading strategy, whereas an apoplasmic translocation step is preferred when photoassimilates cross borders between the maternal-filial generations, or when high concentrations of soluble sugars are being accumulated (Patrick, 1997; Lalonde *et al.*, 2003). However, in many cases plants are not confined to one of the described models of phloem loading and unloading, but rather utilize multiple mechanisms (Knoblauch and Peters, 2013).

After carbohydrates have been released from the phloem, further distribution is necessary. Post-phloem transport can again occur symplasmically and/or apoplasmically. For instance, the pericarp of young tomato berries is supplied symplasmically, while the placenta-seed interface uses an apoplasmic strategy (Ruan and Patrick, 1995; Jin *et al.*, 2009). A similar situation exists in the Arabidopsis seed coat; symplasmic post-phloem transport can supply the outer integument, while the inner integument and the developing embryo are symplasmically isolated and have to be supplied by carrier proteins (Stadler *et al.*, 2005). In the course of grape fruit or potato tuber development, the transport mode switches from symplasmic to

apoplasmic or from apoplasmic to symplasmic, respectively (Viola *et al.*, 2001; Zhang *et al.*, 2006).

Acquiring a detailed understanding of cassava transport and carbohydrate storage is key to identifying targets for biotechnological improvement of cassava yield. In this study, we investigated the mechanisms of carbohydrate allocation from cassava source leaves to starch-storing tuberous roots and the distribution within them. In addition to morphological investigations, we used transgenic *pAtSUC2::GFP* plants, as well as the phloem tracers esculin and 5(6)-carboxyfluorescein diacetate (CFDA) to show that cassava employs an apoplasmic phloem loading and a symplasmic unloading mechanism. We identified vascular rays as important cell files enabling efficient radial post-phloem distribution of sucrose throughout the storage xylem parenchyma in tuberous roots. In addition, enzymatic and proteomic measurements of tuberous root tissues underlined the symplasmic unloading pathway and indicated that starch is stored most efficiently in the outer xylem layers.

## Material and methods

### Plant material and growth conditions

Cassava plants (Cultivars 60444, TME-7, I050128, Z010116) were grown from stem cuttings or tissue culture in a greenhouse in Erlangen, Germany, or in a field at IITA Ibadan, Nigeria. In the greenhouse, a light regime of 12 h light/12 h dark was employed, with a constant temperature of 30 °C and 60% relative humidity.

### Cloning of *pAtSUC2::GFP*

A 946 bp promoter fragment (including the 5' untranslated region (UTR)) upstream of the *AtSUC2* (*At1g22710*) translational start site was amplified from genomic Arabidopsis DNA using the primers *AtSUC2*-fwd: 5'-CACCGAAGACAAGGAGGcatgcaaatagcacacattatg-3' and *AtSUC2*-rev: 5'-CACCGAAGACAACATTatttgacaacaagaagtaag-3' and cloned into the Golden Gate level 0 plasmid pICH41295. The level 1-1f (plasmid pICH47732) *pAtSUC2::GFP*-NOS terminator cassette was created by combining the *AtSUC2* promoter level 0 plasmid with the diffusible green fluorescent protein (GFP) level 0 plasmid pICH41531 and the 3'UTR+NOS terminator level 0 plasmid pICH41421. The level 1-1f plasmid was combined with an endlink 1 plasmid, pICH41722, and the transformation vector p134GG. The p134GG plasmid was created for cassava transformation by introducing Golden Gate compatible ends into a pCambia1301 plasmid and by exchanging the promoter of the *hptII* resistance gene from p35S to pNOS. The plasmids pICH41295, pICH41531, pICH41421, pICH47732, and pICH41722 are part of the modular cloning toolbox for plants described by Engler *et al.* (2014).

### Transformation and screening of transgenic *pAtSUC2::GFP* plants

Cassava genotype 60444 was transformed as described previously (Bull *et al.*, 2009). Transformed plants were screened with RT-PCR and immunoblot (see below). Plants with detected GFP transcript and protein were screened with confocal microscopy for GFP fluorescence. The lines 1239, 1240, 1243, and 1323 were found to display clearly visible GFP fluorescence and were used for this study.

### Histology

Petioles, stems, and roots were dissected by free hand sectioning using razor blades. The samples were transferred to ddH<sub>2</sub>O on microscope slides. To study anatomical structures, sections were stained with a 0.1% (w/v) toluidine blue O (CAS 92-31-9) solution or a freshly prepared, saturated phloroglucinol-HCl solution for 1 min. Propidium iodide staining was performed with a

1.0 mg ml<sup>-1</sup> solution (CAS 25535-16-4). Phloem sieve plates were counter stained with a 1.5% solution of aniline blue (CAS 28631-66-5). Samples were rinsed three times with ddH<sub>2</sub>O until the excess dye was completely removed. The sections were subsequently transferred to ddH<sub>2</sub>O. Lugol staining was performed by incubating the sections in 0.1% aqueous iodide/potassium iodide solution for 15–20 min. Samples were rinsed three times with ddH<sub>2</sub>O until the excess staining solution was completely removed. The sections were subsequently transferred to ddH<sub>2</sub>O.

### Esculin and CFDA loading

To remove the cuticle from source leaves, the leaf surface was gently roughened using sandpaper. 5(6)-Carboxyfluorescein (CF) was loaded into the phloem in its ester form by applying CFDA (CAS 124387-19-5) to the roughened leaf surface. After diluting a CFDA stock solution (10 mg ml<sup>-1</sup> in acetone) 1:5 (v/v) in ddH<sub>2</sub>O, three to four leaves were loaded per plant with 1 ml CFDA each. To avoid evaporation the loaded leaves were covered with parafilm (see Supplementary Fig. S3 at JXB online). Esculin (CAS 531-75-9) was loaded as 10 mg ml<sup>-1</sup> ddH<sub>2</sub>O solution in the same manner as described for CFDA.

### Microscopy

Confocal images were taken on a TCS SP5 (Leica Microsystems CMS GmbH, Mannheim, Germany) using 488 nm laser light for excitation. Detection windows were 499–520 nm (GFP), 654–732 nm (propidium iodide) and 495–515 nm (CF). Light microscopy was using and non-confocal images were taken on a Zeiss Axioskop or a Zeiss STEMI SV11 Stereomicroscope (Zeiss, Wetzlar, Germany). Esculin was excited with a HBO 50 mercury lamp and fluorescence was filtered with a DAPI filter.

### Grafting

Scions of the transgenic *AtSUC2::GFP* line 1240 were grafted onto 4-week-old cassava wild type (WT) rootstocks without tuberous roots. Grafting sites were wrapped with parafilm and plants were kept under elevated humidity for a week. Eight weeks after grafting, plants displayed tuberous roots and these were used for analysis.

### Reverse transcription PCR

RNA was isolated from cassava leaves or roots using the Spectrum Plant Total RNA Kit (Sigma-Aldrich, Taufkirchen, Germany). cDNA was generated using the RevertAid H Minus Reverse Transcriptase as indicated by the manufacturer (Thermo Fisher Scientific, Waltham, MA, USA). Ubiquitin and GFP cDNA was amplified using Taq polymerase and specific oligonucleotide primers (GFP fwd: 5'-ACGTAAACGGCCACAAGTTC-3', GFP rev: 5'-AGTCGTGCTGCTTCATGTG-3'; ubiquitin fwd: 5'-CTCTCACCGCAAGACAATC-3', ubiquitin rev: 5'-CCTCCACGAAGGCGCAG-3').

### Protein PAGE and immunoblot analysis

Total protein extracts were obtained by homogenizing 50 mg frozen leaf or root material in 300 µl of extraction buffer (90 mM Tris-HCl pH 6.8, 20% glycerol, 100 mM DTT, 2% SDS, 0.02% bromophenol blue). Extracts from leaves were heated to 95 °C for 10 min, while extracts from roots were heated to 65 °C for 10 min. Samples were mixed, subjected to 10 min of ultrasonication to shear genomic DNA and centrifuged for 10 min at 15 000 g. The supernatant was loaded on Tris/glycine gels containing 12% acrylamide and subjected to electrophoresis. Blotting of proteins onto nitrocellulose membrane and detection by antibodies (Roche Diagnostics, Mannheim, Germany; Sigma-Aldrich, Taufkirchen, Germany) was carried out as described earlier (Lamm *et al.*, 2017).

### Enzyme activity assays

Storage root extracts were obtained from 100 mg of starting material and treated as described previously (Sonnewald *et al.*, 2012). While the supernatant was used for sucrose synthase activity measurements, the pellet was used to measure cell wall invertase activity as reported earlier (Dancer *et al.*, 1990).

### Measurement of sucrose and starch content

Soluble sugars were extracted from 10 mg of cassava root material as described by [Sonnewald \*et al.\* \(2012\)](#). The starch was extracted from the pellet fraction of the same samples and sucrose and starch content was finally determined enzymatically as described before ([Müller-Röber \*et al.\*, 1992](#)).

### Proteomics

Protein was extracted from each tuberous root sample with 125 µl extraction buffer (100 mM Tris-HCl pH 6.8, 20% glycerol, 100 mM DTT, 2% SDS, 8 M urea, 0.02% bromophenol blue). Extracts were loaded on Tris/glycine SDS-PAGE gels containing 12% acrylamide and subjected to electrophoresis until the proteins entered the separating gel, but were still focused in a single band. Gels were fixed (140 mM 5-sulfosalicylic acid, 1.2 M trichloroacetic acid) and stained with colloidal Coomassie staining solution (960 mM ammonium sulfate, 0.08% Coomassie G 250, 260 mM phosphoric acid, 20% methanol). After destaining (10% acetic acid, 25% methanol) and rinsing in 25% methanol, focused gel bands were cut and subjected to in-gel protein digestion as described by [Shevchenko \*et al.\* \(2006\)](#). Digested peptides were dried and resuspended in 0.5% trifluoroacetic acid and 5% acetonitrile. Peptides were purified using C18 spin columns (Thermo Fisher Scientific), dried and resuspended in 50 mM triethylammonium bicarbonate buffer pH 8.0 and subjected to tandem mass tag labeling as indicated by the manufacturer (Thermo Fisher Scientific). Afterwards, all samples were pooled, dried again and resuspended in 10 mM ammonia and 2% acetonitrile. Prefractionation under alkaline conditions was performed using an UltiMate3000 micro-UHPLC system connected to an autosampler as reported earlier ([Kraner \*et al.\*, 2017](#)). During the 2-h HPLC run, 81 fractions were collected and combined to give 27 fractions. The 27 fractions containing the labeled peptides were dried and resuspended in 10% formic acid and analysed by an Orbitrap Fusion™ Tribrid™ mass spectrometer in connection with an UltiMate3000 nano-UHPLC system. Peptide separation during a 120 min acetonitrile gradient was performed as described earlier ([Kraner \*et al.\*, 2017](#)). MS<sup>3</sup> analyses were performed using the MultiNotch workflow ([McAlister \*et al.\*, 2014](#)). Raw files were analysed using PEAKS Studio 8.5 and the cassava proteome release 6.1 ([Zhang \*et al.\*, 2012](#); [Bredeson \*et al.\*, 2016](#)). Oxidation of methionine residues was set as dynamic modification, while carbamidomethylation of cysteines and labeling with tandem mass tags was set as static modification. A maximum of two missed trypsin cleavage sites was allowed. Parent mass tolerance was set to 10 ppm, fragment mass tolerance was set to 0.5 Da, and TMT quantification mass tolerance was set to 0.8 Da. Relative protein expression was calculated based on the measured TMT reporter ion values in MS<sup>3</sup>. Using these results, further analysis was performed using the Perseus software platform v1.6.2.1 ([Tyanova \*et al.\*, 2016](#)). Expression values were log<sub>2</sub> transformed and proteins were only considered for further analysis when at least two of three replicates yielded values >zero in at least one tissue group. Zero filling was performed using normally distributed values with a downshift of 2.5 and a width of 0.3. In order to identify proteins with significantly different expression over the sample groups, ANOVA and *post hoc* test were performed using a false discovery rate of 0.05. Among all positively identified protein groups, proteins of interest (sucrose synthase (SUS), ADP-glucose pyrophosphorylase small subunit (APS), ADP-glucose pyrophosphorylase large subunit (APL)) were retrieved manually and confirmed by BLASTP as well as Orthofinder software ([Altschul \*et al.\*, 1997, 2005](#); [Emms and Kelly, 2015](#)). The mass spectrometry dataset has been deposited at the ProteomeXchange Consortium via the PRIDE partner repository ([Perez-Riverol \*et al.\*, 2019](#)) with the dataset identifier PXD014001 and 10.6019/PXD014001.

### Determination of phosphorylated intermediates

Measurements of phosphorylated intermediates were performed on 50 mg frozen cassava tissue according to ([Horst \*et al.\*, 2010](#)). The recovery rate for tuberous root tissue was determined prior to analysis by adding known quantities of authentic standards at the start of the metabolite determination process, i.e. the extraction of the metabolites. The recovery rates for fructose-6-phosphate, glucose-6-phosphate, glucose-1-phosphate, and ATP were 92%, 94%, 92%, and 87%, respectively.

## Results and Discussion

### *Cassava storage organs develop specialized cell files for radial transport*

Cassava stem cuttings form two types of adventitious roots, fibrous roots and tuberous roots ([Fig. 1A](#)). The fibrous roots show a typical primary root morphology with a central vascular cylinder surrounded by cortex cells ([Fig. 1B](#)). The central vasculature contains the star-shaped xylem and the phloem tissue. Pericycle and endodermis surround the vasculature. During secondary growth, the xylem enlarges, the vascular cylinder is broken, and the root morphology changes, transforming the fibrous root into a developing tuberous root ([Fig. 1C](#)). The tuberous roots and their neck regions are characterized by the periderm, the phloem tissue, a thin layer of cambium, and a large xylem area ([Fig. 1D, E](#)). Remarkably, a large amount of longitudinal cell files, connecting the phloem and xylem tissue can be observed in cassava tuberous roots ([Fig. 1D, E](#)). These parenchymatic vascular rays were either uniserate or biserate and could already be found in developing tuberous roots, which have just started to undergo secondary growth ([Fig. 1C](#)).

Vascular rays are best known from the stems of wood species, where increasing physical separation of phloem and xylem requires radial solute transport. Here, the rays originate from specialized ray initial cells in the vascular cambium and extend towards both phloem and xylem, thereby connecting the two transport systems. They have important roles in xylem embolism repair, osmotic regulation, long-term carbon storage, as well as seasonal carbon storage and remobilization ([Spicer, 2014](#); [Secchi \*et al.\*, 2017](#); [Furze \*et al.\*, 2018](#)). In deciduous trees of the seasonally dry tropics, starch storage increases prior to the onset of the dry season and there is evidence of mobilization to support leaf flush ([Spicer, 2014](#)). Cassava, as a tropical woody shrub, shows a similar behavior. During the rainy season, the plant grows and stores carbohydrates in stem(s) and tuberous roots, while it arrests growth and sheds most of its leaves during the dry season ([Howeler \*et al.\*, 2013](#)). Stored carbohydrates are remobilized after the dry season to replenish the leaves and continue growth. Therefore, we hypothesize that the vascular rays also play an important role in cassava assimilate transport, carbohydrate storage, and remobilization.

### *Transgenic pAtSUC2::GFP plants show GFP fluorescence along the phloem and vascular rays of tuberous roots*

To study phloem transport, transgenic cassava plants expressing GFP under the control of the Arabidopsis *SUC2* promoter were created. The *AtSUC2* promoter was described as companion cell-specific ([Truernit and Sauer, 1995](#); [Stadler and Sauer, 1996](#); [Imlau \*et al.\*, 1999](#)) and is widely used as a research tool to facilitate phloem-specific expression ([Corbesier \*et al.\*, 2007](#); [Zierer \*et al.\*, 2016](#); [Ross-Elliott \*et al.\*, 2017](#)). Cassava has open collateral vascular bundles with the phloem always on the abaxial side of the xylem. Hence, the xylem is orientated towards the interior and the phloem towards the exterior ([Supplementary Fig. S1](#)). Detailed confocal microscopy analysis of the *pAtSUC2::GFP* plants revealed GFP fluorescence in the

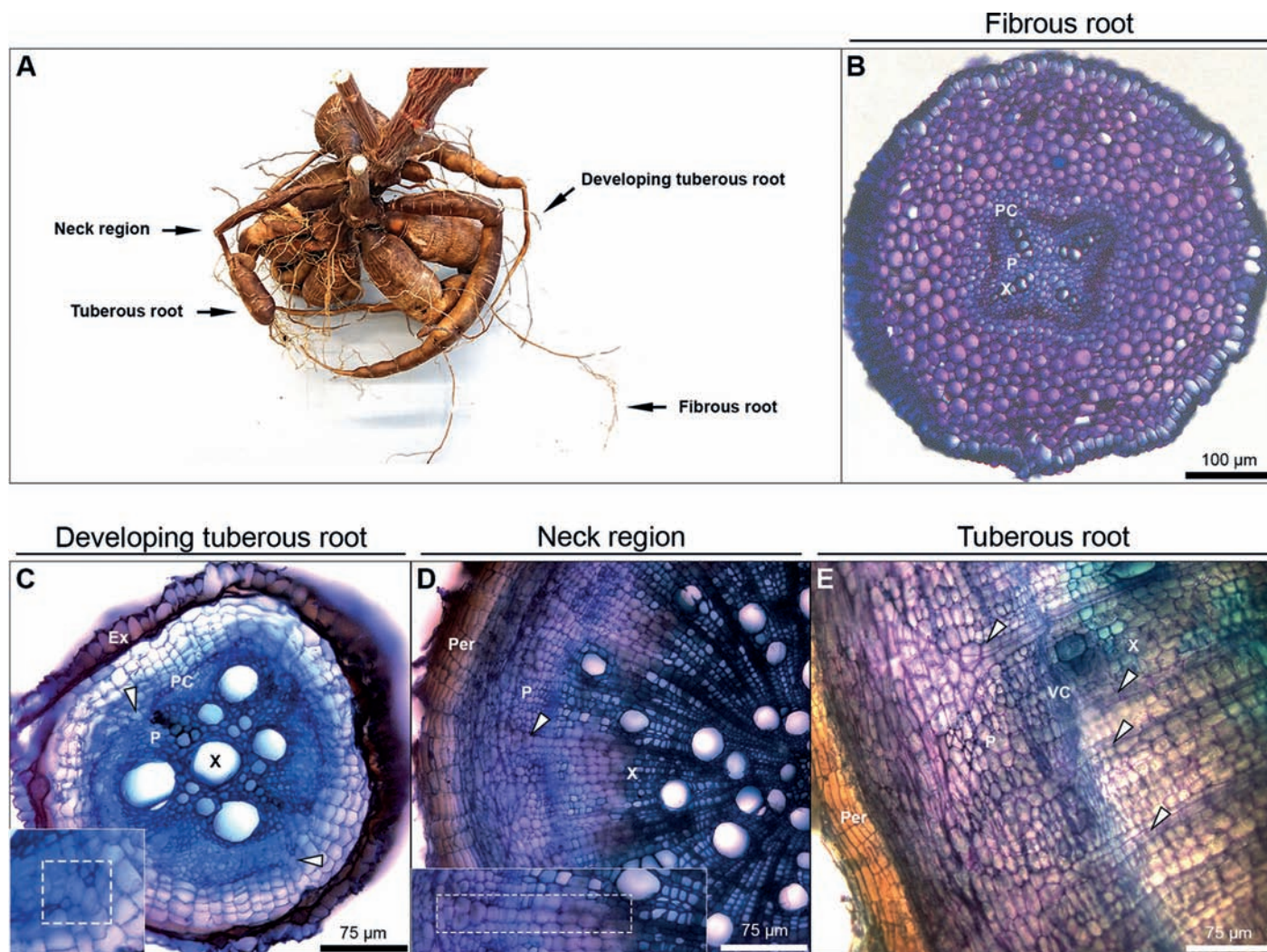


**Fig. 1.** Phloem and xylem cells in tuberous roots of cassava are connected by specialized cell files. (A) Overview of the cassava rootstock. (B) Cross-section of fibrous root. (C) Cross-section of developing tuberous root. Inset shows the breakage of endodermis/pericycle and a structure resembling a newly formed vascular ray. (D) Cross-section of tuberous root neck region. Inset shows an enlarged example of a vascular ray. (E) Cross-section of tuberous root. (B–E) All sections were stained with 0.1% toluidine blue. Ex, exodermis; P, phloem; PC, procambium; Per, periderm; VC, vascular cambium; X, xylem. Arrowheads indicate vascular rays.

petiole phloem (Fig. 2B), stem phloem (Fig. 2E), and tuberous root phloem (Fig. 2H), as well as in parenchymatic vascular rays (Fig. 2H, I). No GFP could be visualized in the leaf or leaf veins (data not shown). GFP signals were always strongest in particular cells with comparable size and regular distribution, likely companion cells or phloem sieve elements (Fig. 2C, F). In the tuberous roots, the strongest GFP signal was detected in the phloem area close to the vascular cambium. GFP fluorescence gradually decreased along the vascular rays towards the xylem, leaving the impression of GFP diffusion. A weaker fluorescence signal, representing a putative diffusion gradient, was visible from the phloem towards the outer tuberous root parts (Fig. 2H). No GFP fluorescence could be observed in WT samples (Fig. 2A, D, G; Supplementary Fig. S2) and GFP fluorescence identity was confirmed by  $\lambda$ -scan (Supplementary Fig. S2). These results indicate that the *AtSUC2* promoter is specifically active along the cassava phloem and that GFP can diffuse into the tuberous root xylem parenchyma through parenchymatic vascular rays.

#### *Transcript and protein analysis indicate movement of GFP from shoot to root*

Characterization of *pAtSUC2::GFP* plants via RT-PCR revealed that GFP transcript could be found in the leaf, major vein, petiole, and root phloem (Fig. 3). Expression in the overall leaf sample was weaker compared with the expression in major vein and petiole, indicating vasculature expression. No GFP expression could be detected in three different, equal-sized xylem fractions, sampled from the outer xylem towards the xylem center (xylem 1–3), containing all xylem cell types, including vascular ray cells. Immunoblot analysis against the GFP protein detected GFP in the leaf, major vein, petiole, and root phloem, as well as in all three xylem fractions. Despite very weak expression of GFP in the root phloem, large amounts of GFP protein could be detected. The xylem fractions displayed decreasing amounts of GFP protein from the outside of the xylem towards the inside. This result underlines the observed gradual distribution of GFP in the tuberous root (Fig. 2H, I) and indicates

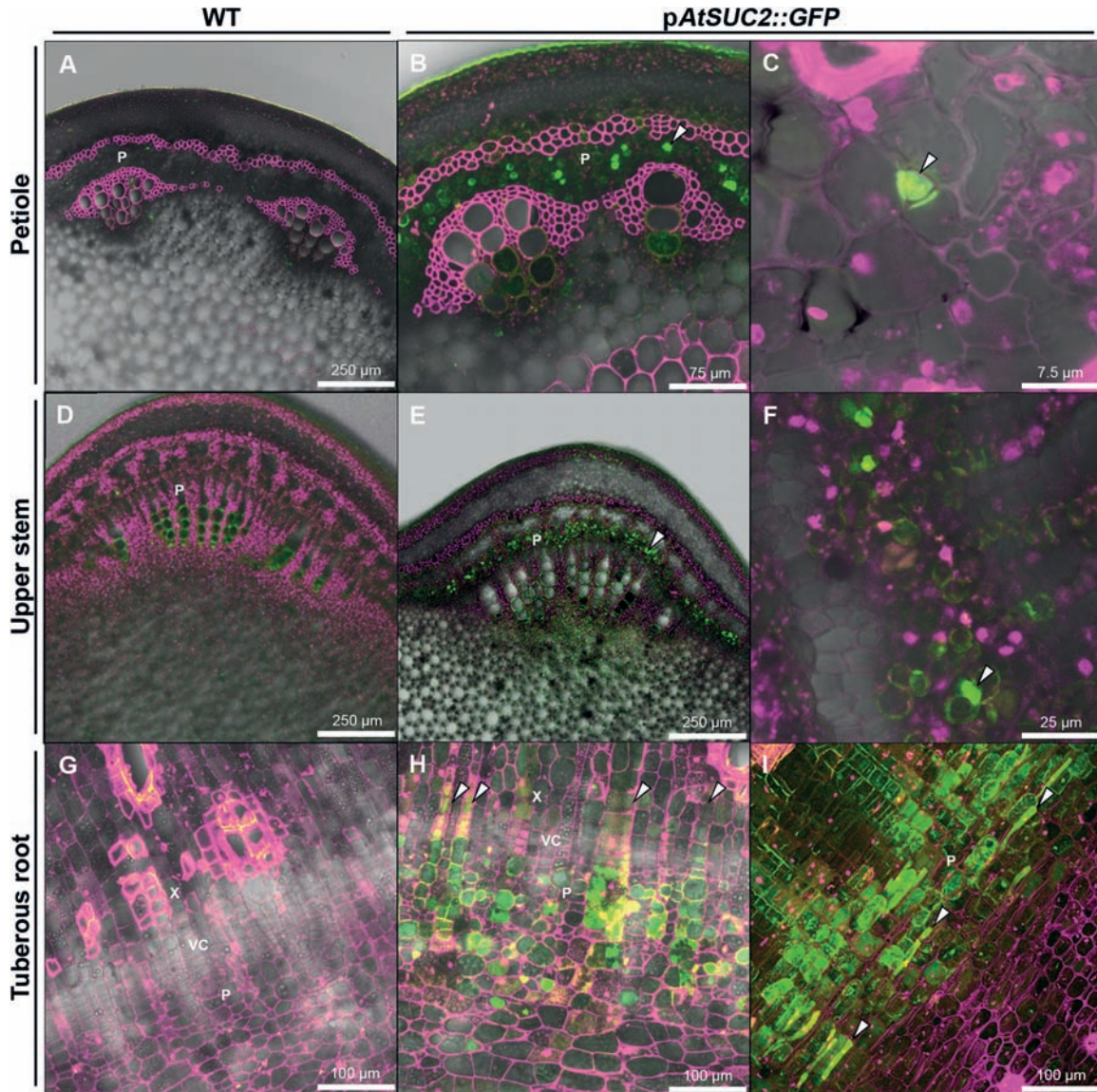


**Fig. 2.** Free GFP can diffuse through parenchymatic vascular rays in cassava tuberous roots. (A) Confocal image of WT petiole cross-section. (B, C) Confocal image of *pAtSUC2::GFP* petiole cross-section. Arrowheads indicate cells with strongest GFP signal. (D) Confocal image of WT upper stem cross-section. (E, F) Confocal image of *pAtSUC2::GFP* upper stem cross-section. Arrowheads indicate cells with strongest GFP signal. (G) Confocal image of WT tuberous root cross-section. (H) Confocal image of *pAtSUC2::GFP* tuberous root cross-section. Arrowheads indicate vascular rays connecting phloem and xylem. (I) Maximum projection of *pAtSUC2::GFP* tuberous root longitudinal section. Arrowheads indicate sieve element-shaped cell files with strongest GFP signal. (A–I) All sections were counterstained with propidium iodide (magenta). All sections were merged with bright field. GFP fluorescence in green. P, phloem; VC, vascular cambium; X, xylem.

transport of GFP from the shoot to the root phloem, with further diffusion through vascular rays towards the root xylem parenchyma. In contrast to the GFP transcript and protein, the GFP fluorescence could not be detected in the leaf veins. However, as the *AtSUC2::GFP* cassava lines are heterozygous T0 events, GFP fluorescence in the *AtSUC2::GFP* plants is overall low and even though it was detectable in the other organs, a combination of low production and GFP transport towards sink organs likely makes GFP hard to visualize in the leaf veins. The detection of GFP transcript and protein in major leaf veins via the more sensitive PCR and immunoblotting techniques suggests that the *AtSUC2* promoter also drives expression and synthesis of GFP protein in the leaf vasculature of cassava, even though it cannot be visualized with the microscope.

Together, the results of the confocal microscopy, transcript, and protein analysis demonstrate that the Arabidopsis *SUC2* promoter mediates phloem-specific expression in cassava and indicates that the GFP protein can move from the shoot phloem to the root, where radial post-phloem transport into the xylem parenchyma is mediated by vascular rays.

#### *Grafting of pAtSUC2::GFP shoots onto WT rootstock proves transport of GFP from the shoot to the root*

To verify transport of GFP from shoot to root directly, we grafted *pAtSUC2::GFP* shoots onto WT rootstock (Fig. 4B). Again, no GFP fluorescence, transcript or protein could be detected in roots of WT plants (Fig. 4A; Supplementary Fig. S3).

The grafted pAtSUC2::GFP shoot still produced GFP and displayed GFP fluorescence specifically in the phloem (Fig. S4A, B; Supplementary Fig. S3). However, 8 weeks after grafting, GFP protein could be detected in newly formed tuberous roots of grafted plants (Supplementary Fig. S3) and GFP fluorescence was strongly detected in the phloem area (Fig. 4C, D). GFP fluorescence was again strongest in the putative CCs/SEs and showed a pronounced gradual distribution along the parenchymatic vascular rays. A weaker gradual distribution could be seen towards the outer phloem parenchyma and periderm cells (Fig. 4D). These results prove that the large 28 kDa GFP is efficiently transported from the shoot to the roots and that it is able to move from the root phloem, where it arrives, towards phloem parenchyma and periderm cells or towards the starch-storing xylem parenchyma. The bulk of GFP seemed to move into the xylem, mediated by vascular rays (Fig. 4D).

### Esculin indicates apoplastic phloem loading

To investigate cassava phloem transport further, the fluorescent sucrose analog esculin was carefully applied to the leaf apoplast

(see Material and methods; Supplementary Fig. S5) and plants were analysed after up to 24 h. Esculin can be transported by SUC/SUT-type carriers and sucrose-specific SWEET carriers and can be imported from the apoplast into the phloem by the phloem loader SUC2 (Knoblauch *et al.*, 2015; Rottmann *et al.*, 2018). In contrast to unloaded WT controls (Fig. 5A), esculin was clearly visible in the esculin-loaded plants (Fig. 5). Cross- and longitudinal sections of petioles showed that esculin was readily taken up and transported along the phloem symplast (Fig. 5B–E). It could be detected, confined to the phloem, at the petiole base 1.5 h after application (not shown). Counterstaining of the phloem sieve plates with aniline blue demonstrated that esculin was transported specifically in sieve elements (Fig. 5E). While unloaded WT plants only showed xylem autofluorescence in the tuberous root (Fig. 5F), esculin-loaded plants displayed strong signal in the phloem and along the vascular rays (Fig. 5G), underlining the results obtained from phloem GFP tracking.

### Vascular rays fulfill a carbohydrate transport and storage function

A second phloem tracer, carboxyfluorescein (CF), was carefully applied in its ester form, CFDA, to the leaf apoplast (see Material and methods; Supplementary Fig. S5). CF has been used to monitor phloem sap flow in several studies (Grignon *et al.*, 1989; Oparka *et al.*, 1994; Knoblauch *et al.*, 2015). In contrast to untreated WT plants (Fig. 6A), CF was clearly visible in the tuberous roots of CFDA-loaded WT plants 24 h after application (Fig. 6B, C). Strong CF signals were again detected in the root phloem area with strong fluorescence gradients along the vascular rays towards the xylem parenchyma and weaker fluorescence gradients towards the phloem parenchyma and periderm, confirming the GFP and esculin results. GFP and the tracers could also be observed in the cells between the rays (Figs 2H, 6B, C; Supplementary Fig. S2A) indicating the presence of plasmodesmata between the rays and the neighboring xylem parenchyma cells. Interestingly, large parts of the cambium seemed to be isolated from the root symplast

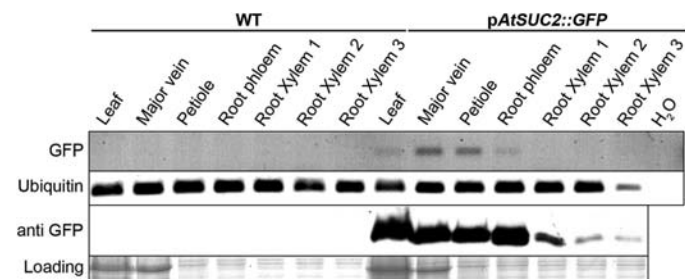


**Fig. 3.** Transgenic pAtSUC2::GFP cassava plants produce GFP in the shoot and translocate it to the roots. Upper lane shows GFP RT-PCR results in different tissues of WT and pAtSUC2::GFP plants. Second lane shows ubiquitin RT-PCR results in different tissues of WT and pAtSUC2::GFP plants. Third lane shows detected GFP protein in different tissues of WT and pAtSUC2::GFP plants via immunoblot using an anti-GFP antibody. Bottom lane shows the loading control in the form of a Coomassie gel with equally loaded protein extract amounts compared with the immunoblot.



**Fig. 4.** Detection of GFP in rootstocks of grafted pAtSUC2::GFP shoots onto WT rootstocks proves movement of GFP from shoot into tuberous roots. (A) Confocal image of WT tuberous root cross-section. (B) pAtSUC2::GFP scion grafted onto WT rootstock. Arrowhead indicates grafting region. (C, D) Confocal image of tuberous root cross-section of pAtSUC2::GFP shoot × WT rootstock grafted plants. Arrowheads indicate vascular rays. (A, C, D) All sections were counterstained with propidium iodide (magenta). All sections are shown with bright field. GFP fluorescence in green. P, phloem; VC, vascular cambium; X, xylem.



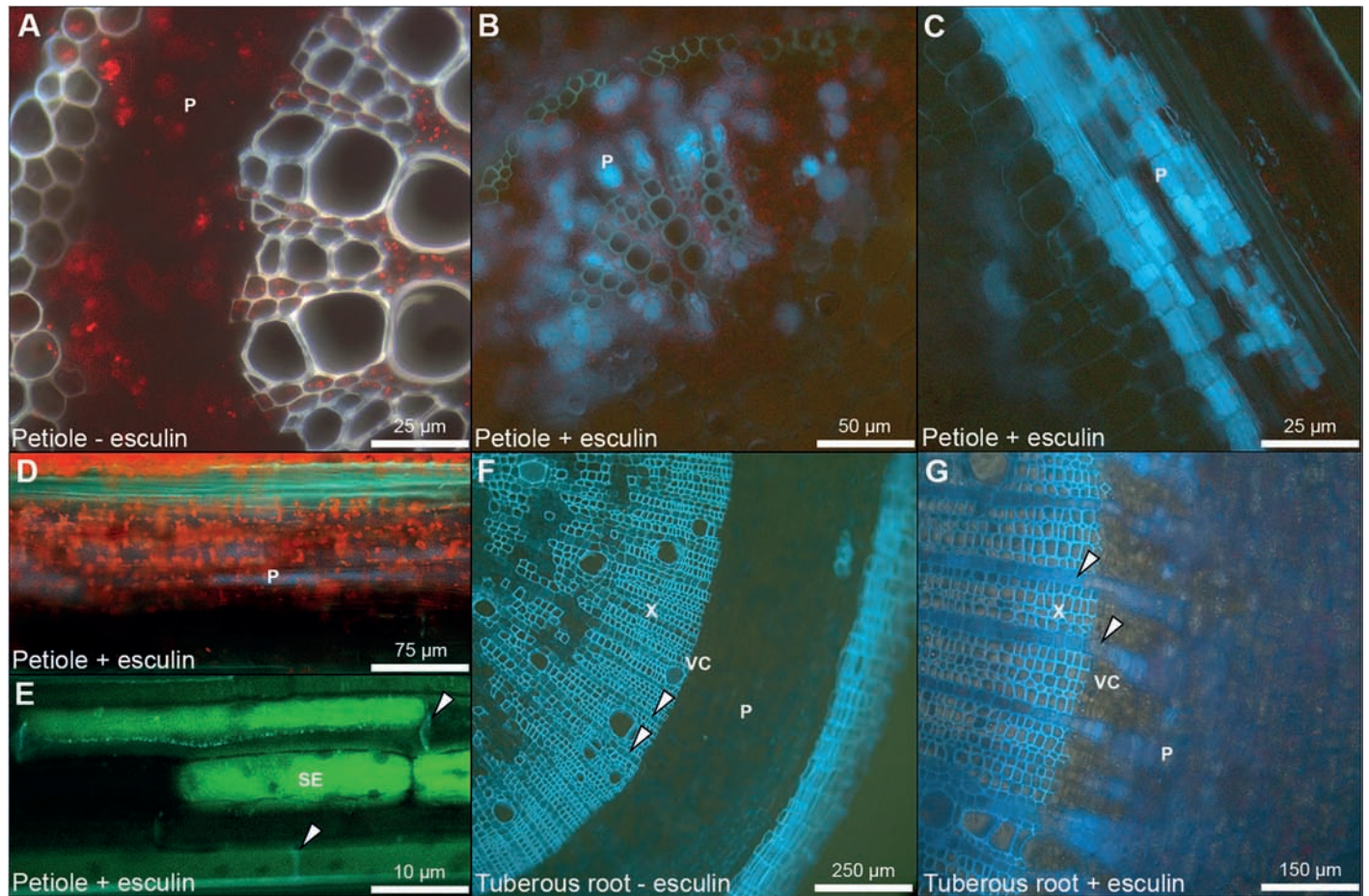


**Fig. 5.** Esculin indicates apoplasmic phloem loading. (A) Autofluorescence in WT petiole. Xylem autofluorescence in white/blue, chlorophyll in red. (B) Fluorescence in petiole cross-section of esculin-loaded WT plant. Esculin in bright light blue, chlorophyll in red. (C, D) Fluorescence in petiole longitudinal section of esculin-loaded WT plant. Esculin in bright light blue, chlorophyll in red. (E) Confocal image of petiole cross-section of esculin-loaded WT plant. Arrowheads indicate sieve plates stained with aniline blue. Esculin fluorescence is displayed in green. (F) Fluorescence in tuberosity root WT cross-section. Xylem autofluorescence in white/light blue. Arrowheads indicate vascular rays. (G) Fluorescence in tuberosity root cross-sections of esculin-loaded WT plant. Xylem autofluorescence in white/light blue, esculin fluorescence in blue. Arrowheads indicate vascular rays. (A–G) P, phloem; SE, sieve element; VC, vascular cambium; X, xylem.

as they always stayed devoid of GFP or tracer substances (Figs 2H, 4D, 5G, 6B, C), which indicates carrier-mediated supply of this tissue. In dicots, the cambium consists of the fusiform and ray initial cells. The fusiform initials are the ultimate progenitors of all classes of xylem and phloem cells, while the ray stem cells initiate the vascular rays, which fulfil transport and storage functions (Van Bel, 1990; Matte Risopatron *et al.*, 2010). Symplasmic isolation of the fusiform cambial cells theoretically allows for better access control and more regulated substance uptake to this important meristematic tissue. Plant sugar levels are spatiotemporally regulated as sugars have numerous effects on plant development. On the one hand, sugars can promote cell division and developmental stage transition (Lastdrager *et al.*, 2014; Wingler, 2018), but on the other hand, high sugar concentrations can also induce meristem quiescence (Lastdrager *et al.*, 2014). More tightly controlled transport via the apoplasmic route into the fusiform cambial cells might therefore be required. Together, the *AtSUC2::GFP* and tracer studies indicate that cassava performs apoplasmic phloem loading and demonstrate symplasmic phloem unloading into

the phloem parenchyma cells of tuberosity roots. Subsequent radial transport towards the starch-storing xylem parenchyma is mediated by vascular rays.

Iodide staining showed that starch is deposited in longitudinal cell files across the tuberosity root (Figs 6D–F; Supplementary Fig. S1L). Especially young, actively storing tuberosity roots revealed strong staining specifically along the vascular rays (Fig. 6E, F), while more developed storage roots showed also intense staining in xylem parenchyma cell files (Figs 6D; Supplementary Fig. S1L). Vascular rays in the wood of trees are known to store starch and the metabolism of the ray cells undergoes cyclic, annual fluctuations. Seasonal storage and remobilization processes in the ray cells correspond with seasonal changes in membrane permeability and cellular organization, reflecting a master system designed to coordinate the carbon balance throughout the year (Van Bel, 1990). Our results indicate that in addition to carbohydrate transport, vascular rays also fulfill an important function in starch storage and potentially in carbohydrate remobilization in cassava.

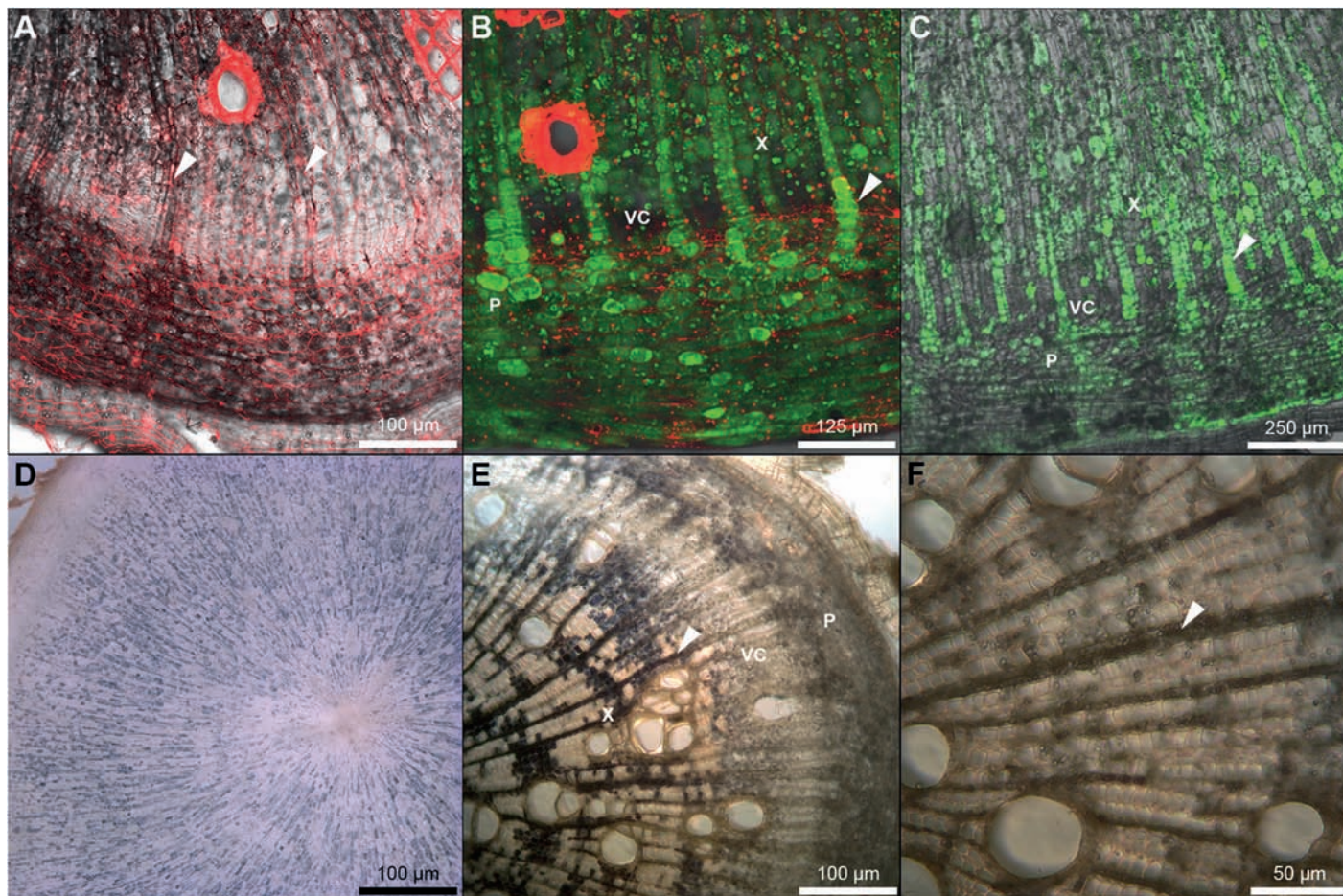


**Fig. 6.** CF monitoring and Lugol staining highlights the importance of vascular rays for carbohydrate transport and storage in tuberous roots. (A) Confocal image with bright field of WT tuberous root cross-section. Propidium iodide in red. (B) Tile-scan picture section of tuberous root cross-section of CFDA-loaded WT plant. Propidium iodide in red, carboxyfluorescein in green. (C) Confocal image with bright field of tuberous root cross-section of CFDA-loaded WT plant. Carboxyfluorescein in green. (D–F) Starch appearing in black/brown after Lugol staining in cross-section of WT tuberous root. Iodide staining in black/brown. (A–F) Arrowheads indicate vascular rays connecting phloem and xylem. P, phloem; VC, vascular cambium; X, xylem.

#### *GFP and CFDA are confined to the fibrous root phloem, while esculin can be unloaded*

To complete the picture of cassava root unloading and post-phloem transport, we also studied unloading in fibrous roots. The analysed fibrous roots showed no signs of secondary growth yet and did not display vascular rays. As expected, the symplasmic tracers GFP (Fig. 7B) and CF (Fig. 7C–F) were confined to the phloem region within the vascular cylinder. Esculin, however, was unloaded from the phloem and taken up by the surrounding root cortex cells (Fig. 7G–I), indicating a transporter-driven phloem unloading of sucrose in fibrous roots. These results support a model in which phloem unloading switches from an apoplasmic mode of transport in fibrous root to a symplasmic mode of transport in tuberous roots, after those have started secondary growth and established parenchymatic vascular rays for phloem–xylem exchange.

#### *Tuberous roots mainly use the sucrolytic pathway for sucrose utilization*

We sectioned tuberous roots of 12-month-old, field grown cassava plants in phloem and six xylem regions (X<sub>1</sub>, outermost xylem region; X<sub>6</sub>, innermost xylem region; Fig. 8A). To get a better understanding

of tuberous root spatial carbohydrate metabolism, we measured sucrose synthase (SUS) activity (Fig. 8B), cell wall invertase (CWI) activity (Fig. 8C) and starch concentrations (Fig. 8D).

Considerable SUS enzyme activity could be measured in the xylem samples. Highest activity with approx. 200 nmol g FW<sup>-1</sup> min<sup>-1</sup> was found in the outermost xylem region of the tuberous roots. SUS enzyme activity gradually decreased towards the center of the tuberous root with approx. 50 nmol g FW<sup>-1</sup> min<sup>-1</sup>. However, no SUS enzyme activity could be measured in the phloem sample, even after treatment with desalting columns or overnight dialysis. Since high levels of secondary metabolites such as cyanogenic glucosides are transported in the cassava phloem (Jørgensen *et al.*, 2005, 2011), the SUS activity could be inhibited in the phloem samples. Mixing xylem extract with increasing amounts of phloem extract indeed resulted in inhibition of the enzyme assay (Supplementary Fig. S6), indicating the presence of an inhibitor in this tissue. Since no SUS antibody was available to us, we performed comparative proteomic analysis on cassava tuberous root phloem and two xylem tissues (outer and inner xylem; Fig. 8E) to ensure that SUS protein was indeed present in those tissues. A targeted search for SUS proteins identified seven variants in all three tissues analysed (Fig. 8F). Compared with the mean expression level of all proteins in

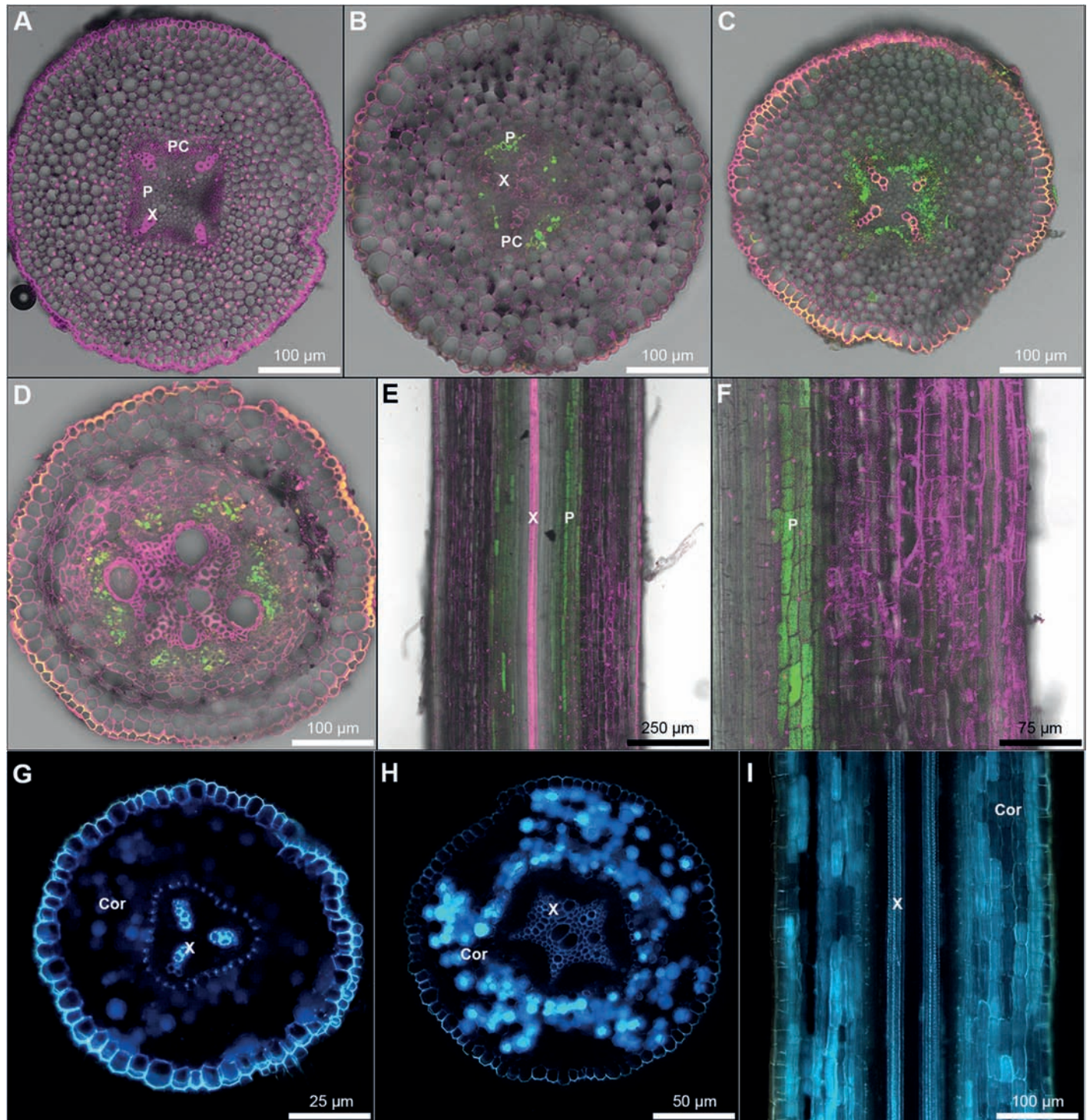


**Fig. 7.** GFP and CF are confined to the fibrous root phloem cell, while esculin can be unloaded. (A) Confocal image of a WT fibrous root cross-section. (B) Confocal image of a *pAtSUC2::GFP* fibrous root cross-section. (C) Confocal image towards the tip of a fibrous root cross-section of a CFDA-loaded WT plant. (D) Confocal image of a fibrous root cross-section of a CFDA-loaded WT plant. (E, F) Confocal image of a fibrous root longitudinal-section of a CFDA-loaded WT plant. (G, H) Fluorescence in fibrous root cross-sections of esculin-loaded plants. Esculin fluorescence in blue, within the cortex area surrounding the vascular cylinder. (I) Fluorescence in fibrous root longitudinal sections of esculin-loaded plants. Esculin fluorescence in blue, within the cortex area outside the vascular cylinder. (A–F) All sections were counterstained with propidium iodide (magenta). All sections are shown with bright field. GFP and CF fluorescence in green. (A–I) Cor, cortex; P, phloem; PC, procambium; X, xylem.

each tissue fraction, three major SUS protein variants showed strong over-representation. Manes.01G221900 (homologous to AtSUS3, At4g02280), Manes.16G090600 (homologous to AtSUS4, At3g43190), and Manes.03G044400 (homologous to

AtSUS1, At5g20830 and AtSUS4, At3g43190) were approx. 60- to 250-fold more abundant than the average protein, while Manes.14G107800, Manes.01G123800, Manes.02G081500, and Manes.03G198900 only showed average protein levels.

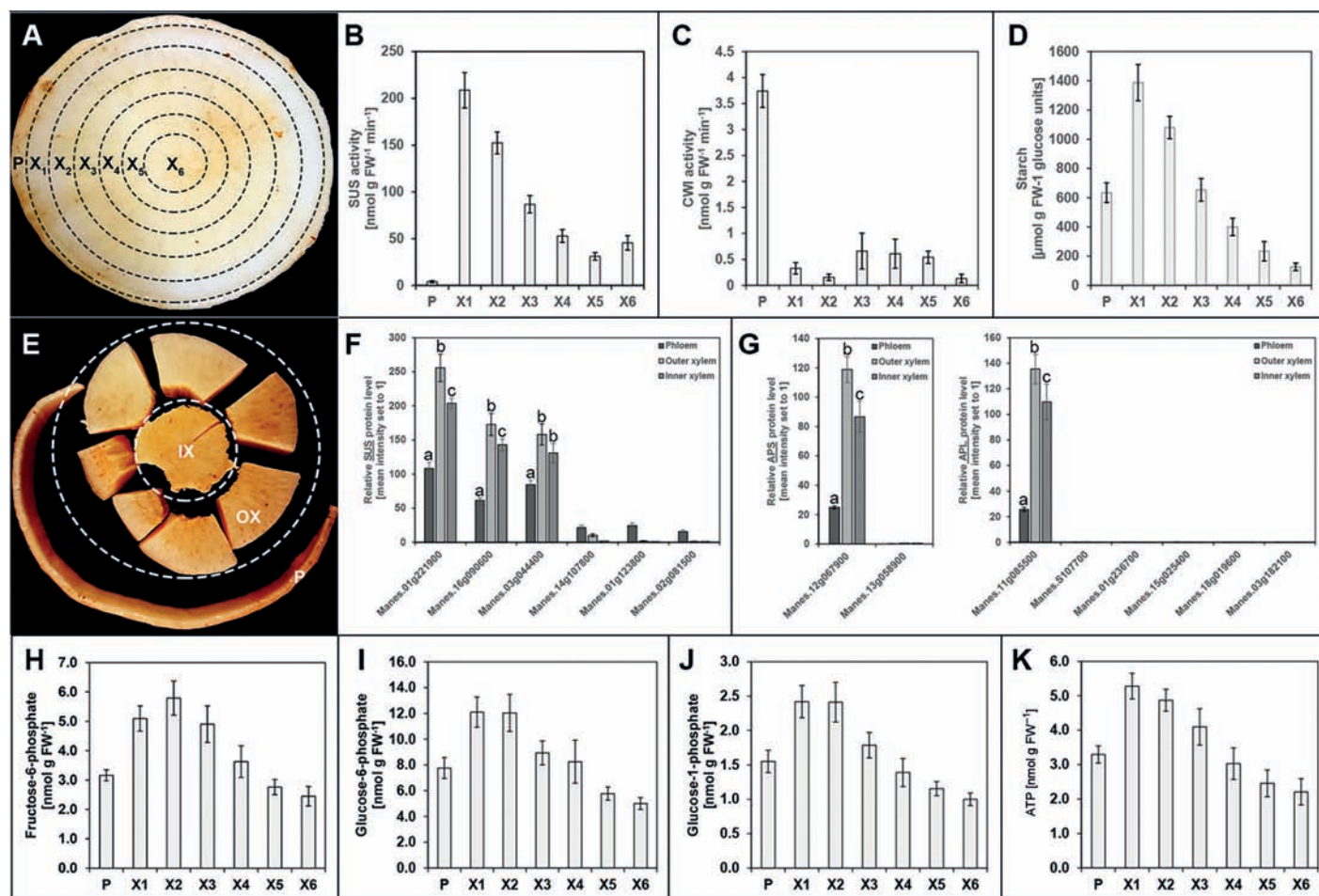


**Fig. 8.** Tuberos roots of cassava mainly use the sucrolytic pathway for starch synthesis and starch is stored most efficiently in the outer xylem. (A) Overview of the sampled tuberous root regions of field-grown cassava genotype Z010116. P, phloem; X<sub>1</sub>–X<sub>6</sub>, xylem fractions 1–6; X<sub>1</sub>, outermost xylem fraction; X<sub>6</sub>, most central xylem fraction. (B) Measured sucrose synthase (SUS) enzyme activity in the phloem and xylem fractions. (C) Measured cell wall invertase (CWI) enzyme activity in the phloem and xylem fractions. (D) Starch concentration in the phloem and xylem fractions. (E) Overview of the sampled tuberous root regions of field-grown cassava genotype I050128 for comparative proteomics. IX, inner xylem; OX, outer xylem; P, phloem and outer root parts. (F) Relative SUS protein levels in phloem, outer xylem and inner xylem samples. Mean intensity determined for each fraction was set to 1. (G) Relative ADP-glucose pyrophosphorylase protein levels in phloem, outer xylem and inner xylem samples. Mean intensity determined for each fraction was set to 1. APL, ADP-glucose pyrophosphorylase large subunit; APS, ADP-glucose pyrophosphorylase small subunit. (H) Fructose-6-phosphate concentration in the phloem and xylem fractions. (I) Glucose-6-phosphate concentration in the phloem and xylem fractions. (J) Glucose-1-phosphate concentration in the phloem and xylem fractions. (K) ATP concentration in the phloem and xylem fractions. (B–D, H–K) Diagrams show the mean of data from  $\geq 4$  biological replicates together with the standard error. (F, G) Diagrams show the mean of data from three biological replicates together with the standard error.

Similar to the SUS enzyme activity distribution, all three proteins displayed the highest abundance in the outer xylem tissue. High abundance of SUS protein could also be detected in the phloem tissue, indicating that sucrose synthase-mediated sucrose cleavage indeed takes place in the phloem but cannot be measured with the enzyme assay used.

In contrast to the high SUS enzymatic activity, the measured cell wall invertase enzymatic activity in the different tuberous root fractions seemed low. The highest activity was found in the phloem sample with approx.  $3.9 \text{ nmol g FW}^{-1} \text{ min}^{-1}$ , while almost no activity could be measured in the different xylem samples (Fig. 8C). The slightly higher activity in the phloem could be the result of a spatially restricted CWI activity. During tuberous root sampling, the outer/phloem region of the tuberous root was peeled off and cell breakage between phloem and xylem occurs in the cambial region (see

for instance Fig. 4C). Tracer experiments indicated apoplasmic supply of the fusiform initial cells of the vascular cambium. If the phloem sample contained cambial cells, this might explain the low but measurable cell wall invertase activity.

Taken together, the results of the enzymatic and proteomic analysis clearly show that tuberous roots have high levels of sucrose synthase protein and enzyme activity.

#### *Sucrose cleavage and starch storage predominantly happens in young xylem parenchyma cells*

Interestingly, the analysis of SUS protein and enzyme activity showed a gradual distribution with highest protein and enzyme activity in the outer layers of the xylem and decreasing levels towards the center of the root. The starch concentration in the different fractions closely followed this pattern.

The concentration was highest in the outermost xylem fraction with approx.  $1400 \mu\text{mol g FW}^{-1}$  glucose units, gradually decreasing towards the center of the root to approx.  $200 \mu\text{mol g FW}^{-1}$  glucose units (Fig. 8D). The phloem region also had a considerable amount of starch at approx.  $700 \mu\text{mol g FW}^{-1}$  glucose units. In addition, the rate-limiting enzyme of starch synthesis, ADP-glucose pyrophosphorylase (Greene and Hannah, 2002), was found to be most abundant in the outer xylem region of the tuberous root (Fig. 8G). Manes.12G067900 and Manes.11G085500 were identified as the major small and large subunit of the ADP-glucose pyrophosphorylase, respectively.

Furthermore, measurements of phosphorylated intermediates showed higher levels for fructose-6-phosphate (Fig. 8H),

glucose-6-phosphate (Fig. 8I), and glucose-1-phosphate (Fig. 8J) in the outer xylem layers and decreasing levels towards the center of the root, likely a consequence of higher sucrose cleavage by sucrose synthase in the outer xylem layers compared with the root center.

Since decreasing sucrose cleavage and starch synthesis towards the center of the root could be linked to ATP shortage, we determined tuberous root ATP levels (Fig. 8K). Indeed, ATP levels across the tuberous root closely followed the pattern observed for SUS protein level, enzymatic activity, starch, and phosphorylated monosaccharides. ATP levels were highest in the outer layers of the xylem and strongly decreased towards the center of the root. The phloem displayed a medium ATP level compared with the different xylem fractions.

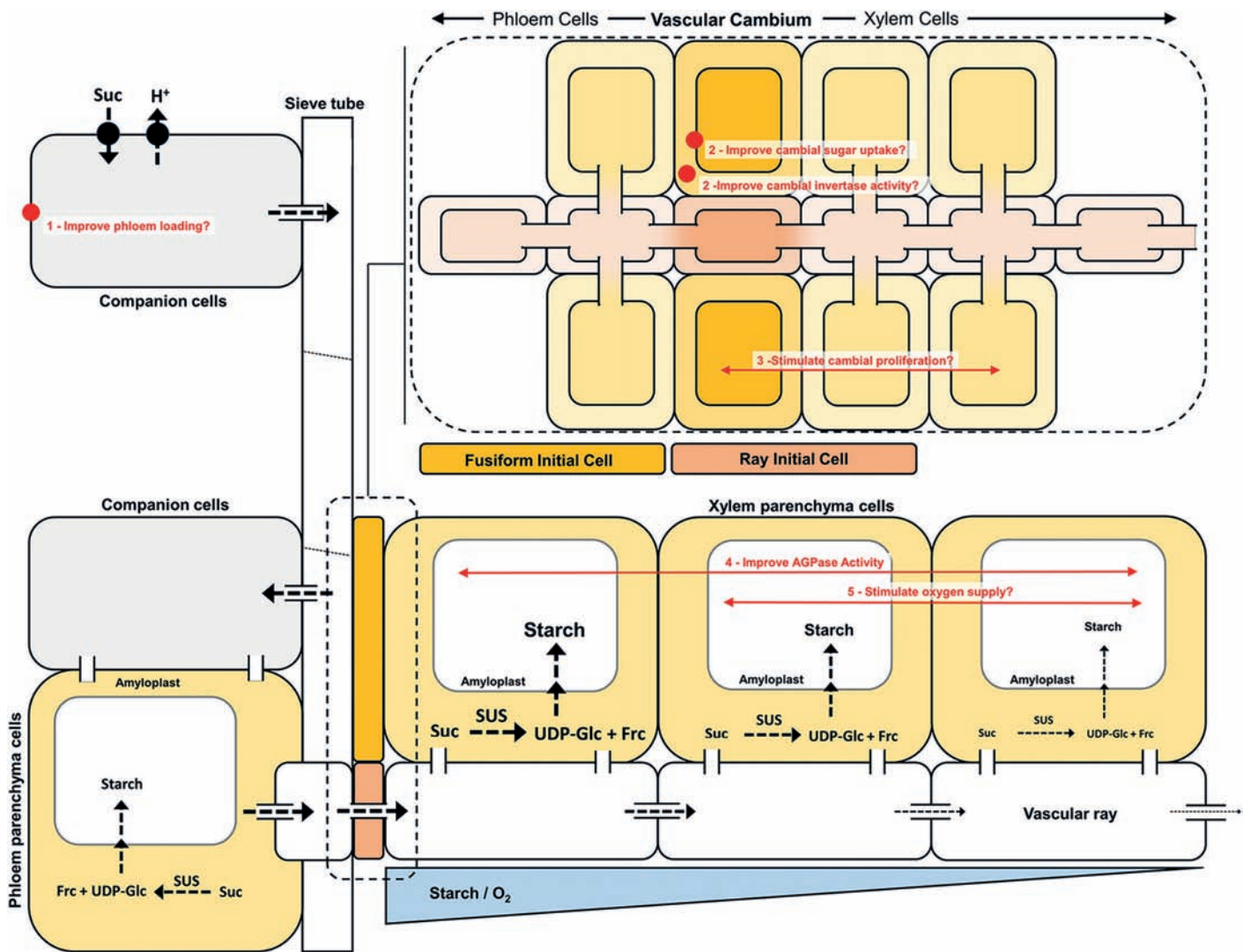


**Fig. 9.** Model of cassava assimilate transport and potential targets for biotechnological yield improvement. Sucrose produced via photosynthesis is transported from the mesophyll cells into the apoplast. Sucrose carriers of the SUC/SUT-family transport sucrose from the apoplast into the phloem companion cell symplast. Sucrose can diffuse through pore plasmodesmal units into the sieve elements for long-distance transport. Sucrose is unloaded via companion cells into the phloem parenchyma cells. Sucrose can diffuse within the phloem and outer parts of the tuberous root; however, the bulk of sucrose diffuses from the phloem towards the xylem parenchyma via vascular rays and is stored as starch. In contrast to the cambial ray initials that are symplasmically connected to phloem and xylem, the fusiform cambial initials are isolated from the tuberous root symplast and likely have to be supplied with sugars through the activity of cell wall invertases and monosaccharide carrier proteins. Potential targets for biotechnological yield improvement are outlined in red and the number corresponds to the following references: 1: Dasgupta *et al.* (2014), Wang *et al.* (2015); 2: Jin *et al.* (2009), Ruan *et al.* (2010); 3: Jang *et al.* (2015), Immanen *et al.* (2016); 4: Ihemere *et al.* (2006); 5: Vigeolas *et al.* (2011). H<sup>+</sup>, proton; Suc, sucrose; SUS, sucrose synthase; UDP-Glc, UDP-glucose.

ATP shortage can be caused by oxygen deficiency as reported, for instance, for potato tubers. Due to poor oxygen distribution throughout roots and tubers, oxygen concentrations can range from 40% to 0% air saturation, depending on the position (Geigenberger *et al.*, 2000; Geigenberger, 2003). Several studies showed that energy-consuming pathways, e.g. starch synthesis, are adjusted to the actual oxygen availability (Bailey-Serres and Voeselek, 2008). Interestingly, cassava root yield is also susceptible to waterlogging (Howeler *et al.*, 2013), which exacerbates oxygen deficiency.

Overall, these results show that sucrose cleavage and starch synthesis in tuberous roots happens most efficiently in the young xylem parenchyma cells.

## Conclusion

In this work, we studied cassava phloem flow by using phloem-specific GFP and the phloem tracers esculin and CFDA, as well as performing proteomic and enzymatic studies on different tuberous root regions. We show that cassava likely employs apoplasmic phloem loading and demonstrate symplasmic phloem unloading into phloem parenchyma cells of tuberous roots. In cassava tuberous roots, radial transport of carbohydrates is facilitated by parenchymatic vascular rays, initiated from ray initial cells of the vascular cambium. In addition to radial solute transport, those rays seem to have a starch storage, and likely, a starch remobilization function. According to our tracer studies, solutes can diffuse from the vascular rays into neighboring xylem parenchyma cells. However, the fusiform initial cells of the vascular cambium seem to be symplasmically isolated from the other root cells, and are likely supplied by invertases and monosaccharide carriers.

Tuberous roots mainly use the sucrolytic pathway for sucrose utilization. Sucrose synthase protein and activity declines from the outer to the inner xylem tissue, which is paralleled by a decreasing starch, phosphorylated monosaccharides, and ATP gradient in the storage xylem parenchyma, indicating decreasing metabolic activity towards the center of the tuberous roots.

Finally, we summarize our current understanding of cassava assimilate transport and outline potential targets for biotechnological improvement of cassava root yield in the model shown in Fig. 9. In brief, we think that improving phloem loading could lead to increased delivery of carbohydrates to tuberous roots and improving tuberous root oxygen supply and ADP-glucose pyrophosphorylase activity could lead to increased starch storage in xylem parenchyma cells. The latter could already be demonstrated in cassava greenhouse experiments (Ihemere *et al.*, 2006). In addition, improving cambial sugar supply or stimulating cambial cell proliferation could be a novel way to increase the root yield of cassava.

## Supplementary data

Supplementary data are available at *JXB* online.

Fig. S1. Overview on cassava petiole, stem, and root morphology.

Fig. S2.  $\lambda$ -Scan of p*AtSUC2::GFP* and WT tuberous roots.

Fig. S3. GFP transcript and protein in p*AtSUC2::GFP* × WT grafted plant.

Fig. S4. Fluorescence in petiole, stem, and tuberous roots of p*AtSUC2::GFP* shoot × WT rootstock.

Fig. S5. Application of esculin or CFDA to a WT 60444 plant.

Fig. S6. Inhibition of SUS enzyme activity by tuberous root phloem tissue.

## Acknowledgements

We thank Ingrid Schieβl, David Pscheidt, Natalie Reinhardt, and Monika Voigt for excellent technical and administrative assistance, respectively. We thank the Bill and Melinda Gates Foundation for funding this research through the grant OPP1113365 'Metabolic Engineering of Carbon Pathways to Enhance Yield of Root and Tuber Crops' provided to Prof. Dr Uwe Sonnewald.

## References

- Altschul SF, Madden TL, Schaffer AA, Zhang J, Zhang Z, Miller W, Lipman DJ. 1997. Gapped BLAST and PSI-BLAST: a new generation of protein database search programs. *Nucleic Acids Research* **25**, 3389–3402.
- Altschul SF, Wootton JC, Gertz EM, Agarwala R, Morgulis A, Schaffer AA, Yu YK. 2005. Protein database searches using compositionally adjusted substitution matrices. *The FEBS Journal* **272**, 5101–5109.
- Arrivault S, Alexandre Moraes T, Obata T, *et al.* 2019. Metabolite profiles reveal interspecific variation in operation of the Calvin–Benson cycle in both C<sub>4</sub> and C<sub>3</sub> plants. *Journal of Experimental Botany* **70**, 1843–1858.
- Bailey-Serres J, Voeselek LA. 2008. Flooding stress: acclimations and genetic diversity. *Annual Review of Plant Biology* **59**, 313–339.
- Braun DM, Wang L, Ruan YL. 2014. Understanding and manipulating sucrose phloem loading, unloading, metabolism, and signalling to enhance crop yield and food security. *Journal of Experimental Botany* **65**, 1713–1735.
- Bredeson JV, Lyons JB, Prochnik SE, *et al.* 2016. Sequencing wild and cultivated cassava and related species reveals extensive interspecific hybridization and genetic diversity. *Nature Biotechnology* **34**, 562–570.
- Bull SE, Owiti JA, Niklaus M, Beeching JR, Grissem W, Vanderschuren H. 2009. *Agrobacterium*-mediated transformation of friable embryogenic calli and regeneration of transgenic cassava. *Nature Protocols* **4**, 1845–1854.
- Bürkle L, Hibberd JM, Quick WP, Kuhn C, Hirner B, Frommer WB. 1998. The H<sup>+</sup>-sucrose cotransporter NtSUT1 is essential for sugar export from tobacco leaves. *Plant Physiology* **118**, 59–68.
- Carvalho LJCB, Filho JF, Anderson JV, Figueiredo PW, Chen S. 2018. Storage root of cassava: morphological types, anatomy, formation, growth, development and harvest time. In: Waisundara V, ed. *Cassava*. London: IntechOpen, 53–68.
- Chaweewan Y, Taylor N. 2015. Anatomical assessment of root formation and tuberization in cassava (*Manihot esculenta* Crantz). *Tropical Plant Biology* **8**, 1–8.
- Chen LQ, Qu XQ, Hou BH, Sosso D, Osorio S, Fernie AR, Frommer WB. 2012. Sucrose efflux mediated by SWEET proteins as a key step for phloem transport. *Science* **335**, 207–211.
- Corbesier L, Vincent C, Jang S, *et al.* 2007. FT protein movement contributes to long-distance signaling in floral induction of *Arabidopsis*. *Science* **316**, 1030–1033.
- Dancer J, Hatzfeld WD, Stitt M. 1990. Cytosolic cycles regulate the turnover of sucrose in heterotrophic cell-suspension cultures of *Chenopodium rubrum* L. *Planta* **182**, 223–231.
- Dasgupta K, Khadilkar AS, Sulpice R, Pant B, Scheible WR, Fisahn J, Stitt M, Ayre BG. 2014. Expression of sucrose transporter cDNAs specifically in companion cells enhances phloem loading and long-distance transport of sucrose but leads to an inhibition of growth and the perception of a phosphate limitation. *Plant Physiology* **165**, 715–731.

- De Schepper V, De Swaef T, Bauweraerts I, Steppe K.** 2013. Phloem transport: a review of mechanisms and controls. *Journal of Experimental Botany* **64**, 4839–4850.
- De Souza AP, Long SP.** 2018. Toward improving photosynthesis in cassava: characterizing photosynthetic limitations in four current African cultivars. *Food and Energy Security* **7**, e00130.
- De Souza AP, Massenburg LN, Jaiswal D, Cheng S, Shekar R, Long SP.** 2017. Rooting for cassava: insights into photosynthesis and associated physiology as a route to improve yield potential. *New Phytologist* **213**, 50–65.
- Emms DM, Kelly S.** 2015. OrthoFinder: solving fundamental biases in whole genome comparisons dramatically improves orthogroup inference accuracy. *Genome Biology* **16**, 157.
- Engler C, Youles M, Gruetzner R, Ehnert TM, Werner S, Jones JD, Patron NJ, Marillonnet S.** 2014. A golden gate modular cloning toolbox for plants. *ACS Synthetic Biology* **3**, 839–843.
- Fu Q, Cheng L, Guo Y, Turgeon R.** 2011. Phloem loading strategies and water relations in trees and herbaceous plants. *Plant Physiology* **157**, 1518–1527.
- Furze ME, Trumbore S, Hartmann H.** 2018. Detours on the phloem sugar highway: stem carbon storage and remobilization. *Current Opinion in Plant Biology* **43**, 89–95.
- Geigenberger P.** 2003. Regulation of sucrose to starch conversion in growing potato tubers. *Journal of Experimental Botany* **54**, 457–465.
- Geigenberger P, Fernie AR, Gibon Y, Christ M, Stitt M.** 2000. Metabolic activity decreases as an adaptive response to low internal oxygen in growing potato tubers. *Biological Chemistry* **381**, 723–740.
- Giaquinta R.** 1977. Phloem loading of sucrose: pH dependence and selectivity. *Plant Physiology* **59**, 750–755.
- Greene TW, Hannah LC.** 2002. Adenosine diphosphate glucose pyrophosphorylase, a rate-limiting step in starch biosynthesis. *Physiologia Plantarum* **103**, 574–580.
- Grignon N, Touraine B, Durand M.** 1989. 6(5)Carboxyfluorescein as a tracer of phloem sap translocation. *American Journal of Botany* **76**, 871–877.
- Hershey C, Álvarez E, Aye TM, et al.** 2012. Eco-efficient interventions to support cassava's multiple roles in improving the lives of smallholders. In: Hershey CH, Neate P, ed. *Eco-efficiency: from vision to reality*. Cali, Colombia: International Center for Tropical Agriculture (CIAT), 135–160.
- Horst RJ, Doehlemann G, Wahl R, Hofmann J, Schmiedl A, Kahmann R, Kämper J, Sonnewald U, Voll LM.** 2010. *Ustilago maydis* infection strongly alters organic nitrogen allocation in maize and stimulates productivity of systemic source leaves. *Plant Physiology* **152**, 293–308.
- Howeler R, Litaladio N, Thomas G.** 2013. *Save and grow: cassava. A guide to sustainable production intensification*. Rome: Food and Agriculture Organization of the United Nations.
- Ihemere U, Arias-Garzon D, Lawrence S, Sayre R.** 2006. Genetic modification of cassava for enhanced starch production. *Plant Biotechnology Journal* **4**, 453–465.
- Imlau A, Truernit E, Sauer N.** 1999. Cell-to-cell and long-distance trafficking of the green fluorescent protein in the phloem and symplastic unloading of the protein into sink tissues. *The Plant Cell* **11**, 309–322.
- Immanen J, Nieminen K, Smolander OP, et al.** 2016. Cytokinin and auxin display distinct but interconnected distribution and signaling profiles to stimulate cambial activity. *Current Biology* **26**, 1990–1997.
- Jang G, Lee JH, Rastogi K, Park S, Oh SH, Lee JY.** 2015. Cytokinin-dependent secondary growth determines root biomass in radish (*Raphanus sativus* L.). *Journal of Experimental Botany* **66**, 4607–4619.
- Jarvis A, Ramirez-Villegas J, Herrera Campo BV, Navarro-Racines C.** 2012. Is cassava the answer to African climate change adaptation? *Tropical Plant Biology* **5**, 9–29.
- Jin Y, Ni DA, Ruan YL.** 2009. Posttranslational elevation of cell wall invertase activity by silencing its inhibitor in tomato delays leaf senescence and increases seed weight and fruit hexose level. *The Plant Cell* **21**, 2072–2089.
- Jørgensen K, Bak S, Busk PK, Sørensen C, Olsen CE, Puonti-Kaerlas J, Møller BL.** 2005. Cassava plants with a depleted cyanogenic glucoside content in leaves and tubers. Distribution of cyanogenic glucosides, their site of synthesis and transport, and blockage of the biosynthesis by RNA interference technology. *Plant Physiology* **139**, 363–374.
- Jørgensen K, Morant AV, Morant M, Jensen NB, Olsen CE, Kannangara R, Motawia MS, Møller BL, Bak S.** 2011. Biosynthesis of the cyanogenic glucosides linamarin and lotaustralin in cassava: isolation, biochemical characterization, and expression pattern of CYP71E7, the oxime-metabolizing cytochrome P450 enzyme. *Plant Physiology* **155**, 282–292.
- Kehr J, Kragler F.** 2018. Long distance RNA movement. *New Phytologist* **218**, 29–40.
- Knoblauch M, Knoblauch J, Mullendore DL, Savage JA, Babst BA, Beecher SD, Dodgen AC, Jensen KH, Holbrook NM.** 2016. Testing the Münch hypothesis of long distance phloem transport in plants. *eLife* **5**, e15341.
- Knoblauch M, Peters WS.** 2013. Long-distance translocation of photosynthates: a primer. *Photosynthesis Research* **117**, 189–196.
- Knoblauch M, Vendrell M, de Leau E, Paterlini A, Knox K, Ross-Elliott T, Reinders A, Brockman SA, Ward J, Oparka K.** 2015. Multispectral phloem-mobile probes: properties and applications. *Plant Physiology* **167**, 1211–1220.
- Kraner ME, Müller C, Sonnewald U.** 2017. Comparative proteomic profiling of the choline transporter-like1 (CHER1) mutant provides insights into plasmodesmata composition of fully developed *Arabidopsis thaliana* leaves. *The Plant Journal* **92**, 696–709.
- Lalonde S, Tegeder M, Throne-Holst M, Frommer WB, Patrick JW.** 2003. Phloem loading and unloading of sugars and amino acids. *Plant, Cell & Environment* **26**, 37–56.
- Lamm CE, Kraner ME, Hofmann J, Börnke F, Mock HP, Sonnewald U.** 2017. Hop/Sti1 – a two-faced cochaperone involved in pattern recognition receptor maturation and viral infection. *Frontiers in Plant Science* **8**, 1754.
- Lastdrager J, Hanson J, Smeekens S.** 2014. Sugar signals and the control of plant growth and development. *Journal of Experimental Botany* **65**, 799–807.
- Lucas WJ, Groover A, Lichtenberger R, et al.** 2013. The plant vascular system: evolution, development and functions. *Journal of Integrative Plant Biology* **55**, 294–388.
- Matte Risopatron JP, Sun Y, Jones BJ.** 2010. The vascular cambium: molecular control of cellular structure. *Protoplasma* **247**, 145–161.
- McAlister GC, Nusinow DP, Jedrychowski MP, Wühr M, Huttlin EL, Erickson BK, Rad R, Haas W, Gygi SP.** 2014. MultiNotch MS3 enables accurate, sensitive, and multiplexed detection of differential expression across cancer cell line proteomes. *Analytical Chemistry* **86**, 7150–7158.
- Milne RJ, Offler CE, Patrick JW, Grof CPL.** 2015. Cellular pathways of source leaf phloem loading and phloem unloading in developing stems of *Sorghum bicolor* in relation to stem sucrose storage. *Functional Plant Biology* **42**, 957–970.
- Milne RJ, Perroux JM, Rae AL, Reinders A, Ward JM, Offler CE, Patrick JW, Grof CP.** 2017. Sucrose transporter localization and function in phloem unloading in developing stems. *Plant Physiology* **173**, 1330–1341.
- Müller-Röber B, Sonnewald U, Willmitzer L.** 1992. Inhibition of the ADP-glucose pyrophosphorylase in transgenic potatoes leads to sugar-storing tubers and influences tuber formation and expression of tuber storage protein genes. *The EMBO Journal* **11**, 1229–1238.
- Münch E.** 1930. *Die Stoffbewegungen in der Pflanze*. Jena: Gustav Fischer.
- Okamoto S, Tabata R, Matsubayashi Y.** 2016. Long-distance peptide signaling essential for nutrient homeostasis in plants. *Current Opinion in Plant Biology* **34**, 35–40.
- Olsen KM, Schaal BA.** 1999. Evidence on the origin of cassava: phylogeography of *Manihot esculenta*. *Proceedings of the National Academy of Sciences, USA* **96**, 5586–5591.
- Oparka KJ, Duckett CM, Prior DAM, Fisher DB.** 1994. Real-time imaging of phloem unloading in the root tip of *Arabidopsis*. *The Plant Journal* **6**, 759–766.
- Patrick JW.** 1997. Phloem unloading: sieve element unloading and post-sieve element transport. *Annual Review of Plant Physiology and Plant Molecular Biology* **48**, 191–222.
- Perez-Riverol Y, Csordas A, Bai J, et al.** 2019. The PRIDE database and related tools and resources in 2019: improving support for quantification data. *Nucleic Acids Research* **47**, D442–D450.
- Rennie EA, Turgeon R.** 2009. A comprehensive picture of phloem loading strategies. *Proceedings of the National Academy of Sciences, USA* **106**, 14162–14167.

- Riesmeier JW, Willmitzer L, Frommer WB.** 1994. Evidence for an essential role of the sucrose transporter in phloem loading and assimilate partitioning. *The EMBO Journal* **13**, 1–7.
- Ross-Elliott TJ, Jensen KH, Haaning KS, et al.** 2017. Phloem unloading in *Arabidopsis* roots is convective and regulated by the phloem-pole pericycle. *eLife* **6**, e24125.
- Rottmann TM, Fritz C, Lauter A, Schneider S, Fischer C, Danzberger N, Dietrich P, Sauer N, Stadler R.** 2018. Protoplast-esculin assay as a new method to assay plant sucrose transporters: characterization of AtSUC6 and AtSUC7 sucrose uptake activity in *Arabidopsis* Col-0 ecotype. *Frontiers in Plant Science* **9**, 430.
- Ruan YL, Jin Y, Yang YJ, Li GJ, Boyer JS.** 2010. Sugar input, metabolism, and signaling mediated by invertase: roles in development, yield potential, and response to drought and heat. *Molecular Plant* **3**, 942–955.
- Ruan YL, Patrick JW.** 1995. The cellular pathway of postphloem sugar transport in developing tomato fruit. *Planta* **196**, 434–444.
- Secchi F, Pagliarani C, Zwieniecki MA.** 2017. The functional role of xylem parenchyma cells and aquaporins during recovery from severe water stress. *Plant, Cell & Environment* **40**, 858–871.
- Shevchenko A, Tomas H, Havlis J, Olsen JV, Mann M.** 2006. In-gel digestion for mass spectrometric characterization of proteins and proteomes. *Nature Protocols* **1**, 2856–2860.
- Sonnewald S, Priller JP, Schuster J, Glickmann E, Hajirezaei MR, Siebig S, Mudgett MB, Sonnewald U.** 2012. Regulation of cell wall-bound invertase in pepper leaves by *Xanthomonas campestris* pv. *vesicatoria* type three effectors. *PLoS One* **7**, e51763.
- Spicer R.** 2014. Symplasmic networks in secondary vascular tissues: parenchyma distribution and activity supporting long-distance transport. *Journal of Experimental Botany* **65**, 1829–1848.
- Stadler R, Lauterbach C, Sauer N.** 2005. Cell-to-cell movement of green fluorescent protein reveals post-phloem transport in the outer integument and identifies symplastic domains in *Arabidopsis* seeds and embryos. *Plant Physiology* **139**, 701–712.
- Stadler R, Sauer N.** 1996. The *Arabidopsis thaliana* AtSUC2 gene is specifically expressed in companion cells. *Botanica Acta* **109**, 299–306.
- Truernit E, Sauer N.** 1995. The promoter of the *Arabidopsis thaliana* SUC2 sucrose-H<sup>+</sup> symporter gene directs expression of  $\beta$ -glucuronidase to the phloem: evidence for phloem loading and unloading by SUC2. *Planta* **196**, 564–570.
- Turgeon R.** 1996. Phloem loading and plasmodesmata. *Trends in Plant Science* **1**, 418–423.
- Turgeon R, Medville R.** 1998. The absence of phloem loading in willow leaves. *Proceedings of the National Academy of Sciences, USA* **95**, 12055–12060.
- Turgeon R, Wolf S.** 2009. Phloem transport: cellular pathways and molecular trafficking. *Annual Review of Plant Biology* **60**, 207–221.
- Tyanova S, Temu T, Sinitcyn P, Carlson A, Hein MY, Geiger T, Mann M, Cox J.** 2016. The Perseus computational platform for comprehensive analysis of (prote)omics data. *Nature Methods* **13**, 731–740.
- Van Bel AJE.** 1990. Xylem–phloem exchange via the rays: the undervalued route of transport. *Journal of Experimental Botany* **41**, 631–644.
- Van Bel AJE.** 2003. The phloem, a miracle of ingenuity. *Plant, Cell and Environment* **26**, 125–149.
- Van Bel AJE, Kempers R.** 1997. The pore/plasmodesm unit; key element in the interplay between sieve element and companion cell. *Progress in Botany* **58**, 278–291.
- Vigeolas H, Hühn D, Geigenberger P.** 2011. Nonsymbiotic hemoglobin-2 leads to an elevated energy state and to a combined increase in polyunsaturated fatty acids and total oil content when overexpressed in developing seeds of transgenic *Arabidopsis* plants. *Plant Physiology* **155**, 1435–1444.
- Viola R, Roberts AG, Haupt S, Gazzani S, Hancock RD, Marmiroli N, Machray GC, Oparka KJ.** 2001. Tuberization in potato involves a switch from apoplastic to symplastic phloem unloading. *The Plant Cell* **13**, 385–398.
- Wang L, Lu Q, Wen X, Lu C.** 2015. Enhanced sucrose loading improves rice yield by increasing grain size. *Plant Physiology* **169**, 2848–2862.
- Wingler A.** 2018. Transitioning to the next phase: the role of sugar signaling throughout the plant life cycle. *Plant Physiology* **176**, 1075–1084.
- Zhang J, Xin L, Shan B, Chen W, Xie M, Yuen D, Zhang W, Zhang Z, Lajoie GA, Ma B.** 2012. PEAKS DB: *de novo* sequencing assisted database search for sensitive and accurate peptide identification. *Molecular & Cellular Proteomics* **11**, M111.010587.
- Zhang XY, Wang XL, Wang XF, Xia GH, Pan QH, Fan RC, Wu FQ, Yu XC, Zhang DP.** 2006. A shift of Phloem unloading from symplasmic to apoplastic pathway is involved in developmental onset of ripening in grape berry. *Plant Physiology* **142**, 220–232.
- Zierer W, Hajirezaei MR, Eggert K, Sauer N, von Wirén N, Pommerrenig B.** 2016. Phloem-specific methionine recycling fuels polyamine biosynthesis in a sulfur-dependent manner and promotes flower and seed development. *Plant Physiology* **170**, 790–806.